Inorg. Chem. **2009**, *48*, 1223−1231

Phosphine Polymerization by Nitric Oxide: Experimental Characterization and Theoretical Predictions of Mechanism

Yi-Lei Zhao,*,† Jason W. Flora,‡ William David Thweatt,‡ Stephen L. Garrison,† Carlos Gonzalez,*,† K. N. Houk,§ and Manuel Marquez*,†,||

NIST Center for Theoretical and Computational Nanosciences, Physical and Chemical Properties Division, Gaithersburg, Maryland 20899, Altria Client Services, Research Development and Engineering, 601 E. Jackson Street, Richmond, Virginia 23219, Department of Chemistry and Biochemistry, University of California, Los Angeles, California 90095, and Harrington Department Bioengineering, Arizona State University, Tempe, Arizona 85287 and Center for Integrated Nanotechnologies, Los Alamos National Laboratory, Los Alamos, New Mexico 87545

Received October 8, 2008

A yellow solid material [P_xH_y] has been obtained in the reaction of phosphine (PH_3) and nitric oxide (NO) at room temperature and characterized by thermogravimetric analysis mass spectrometry (TGA-MS) and attenuated total reflection Fourier transform infrared (ATR-FTIR) spectroscopy. In this work using complete basis set (CBS-QB3) methods a plausible mechanism has been investigated for phosphine polymerization in the presence of nitric oxide (NO). Theoretical explorations with the ab initio method suggest (a) instead of the monomer the nitric oxide dimer acts as an initial oxidant, (b) the resulting phosphine oxides ($H_3P{=}O \leftrightarrow H_3P^+O^-$) in the gas phase draw each other via strong dipolar interactions between the P−O groups, and (c) consequently an autocatalyzed polymerization occurs among the phosphine oxides, forming P−P chemical bonds and losing water. The possible structures of polyhydride phosphorus polymer were discussed. In the calculations a series of cluster models was computed to simulate polymerization.

Introduction

Allotropic carbons and hydrocarbon polymers, such as diamond, graphite, fullerenes, carbon nanotubes, polyacetylene, polyethylene, and polystyrene, have drawn scientists' attention for centuries due to their rich structural diversity and multiple applications in modern industries. Similarly, elemental phosphorus has long been known to possess a wide variety of allotropic forms and structures that can be functionalized.[1−4] For example, simply controlled defect formation in certain allotropic phosphorus materials can change the chemical reactivity of hydrolysis.[5]

However, synthesis of compounds containing P−P bonds has proven to be much more challenging than synthesis of their carbon cousins.[6] Thus, formation of P−P bonds by means of conventional chemical syntheses using organic phosphine monomers[7−11] requires carefully tuning the reaction conditions to harness formation of P−P compounds.

* To whom correspondence should be addressed. E-mail: yi-lei.zhao@nist.gov.
† NIST Center for Theoretical and Computational Nanosciences.
‡ Altria Client Services.
§ University of California, Los Angeles.
|| Arizona State University and Los Alamos National Laboratory.

(1) Bocker, S.; Haser, M. *Z. Anorg. Allg. Chem.* **1995**, *621* (2), 258–286.
(2) Ruck, M.; Hoppe, D.; Wahl, B.; Simon, P.; Wang, Y. K.; Seifert, G. *Angew. Chem., Int. Ed.* **2005**, *44* (46), 7616–7619.
(3) Pfitzner, A. *Angew. Chem., Int. Ed.* **2006**, *45* (5), 699–700.
(4) Pfitzner, A.; Brau, M. F.; Zweck, J.; Brunklaus, G.; Eckert, H. *Angew. Chem., Int. Ed.* **2004**, *43* (32), 4228–4231.
(5) Sukhov, B. G.; Gusarova, N. K.; Malysheva, S. F.; Trofimov, B. A. *Russ. Chem. Bull.* **2003**, *52* (6), 1239–1252.
(6) (a) Masuda, J. D.; Schoeller, W. W.; Donnadieu, B.; Bertrand, G. *Angew. Chem., Int. Ed.* **2007**, *46* (37), 7052–7055. (b) Masuda, J. D.; Schoeller, W. W.; Donnadieu, B.; Bertrand, G. *J. Am. Chem. Soc.* **2007**, *129* (46), 14180–14181. (c) Dyker, C. A.; Bertrand, G. *Science* **2008**, *321* (5892), 1050–1051.
(7) (a) Burford, N.; Ragogna, P. J.; McDonald, R.; Ferguson, M. J. *J. Am. Chem. Soc.* **2003**, *125* (47), 14404–14410. (b) Antoniotti, P.; Operti, L.; Rabezzana, R.; Tonachini, G.; Vaglio, G. A. *J. Chem. Phys.* **2000**, *112* (4), 1814–1822.
(8) Baudler, M.; Eickmans, K. S. *Z. Anorg. Allg. Chem.* **2001**, *627* (8), 1824–1827.
(9) Baudler, M.; Michels, A.; Michels, M. *Z. Anorg. Allg. Chem.* **2001**, *627* (1), 31–36.
(10) Wiberg, E.; Ghemen, M. v.; Müller-Schiedmayer, G. *Angew. Chem., Int. Ed.* **1963**, *75* (18), 814–823.
(11) Langhans, K. P.; Stelzer, O.; Svara, J.; Weferling, N. *Z. Naturforsch. Sect. B: J. Chem. Sci.* **1990**, *45* (2), 203–211.

10.1021/ic801917a CCC: $40.75
Published on Web 12/22/2008

Otherwise, undesired products, such as oxyacids and phosphorus oxides, will be obtained.[8,9,12]

Chemically stable P−P compounds remain elusive. Under ambient conditions most small phosphorus and hydrophosphorus (phosphorus hydride) molecules (P_4, P_2H_4, and P_4H_6) are rapidly oxidized by oxygen at room temperature. On the other hand, some allotropic forms of phosphorus such as black and red phosphorus [P_n] hardly degrade in air and water.

Nitric oxide oxidizes organic phosphines to produce their corresponding phosphine oxides ($R_3P{=}O$, R = phenyl, halogen) and nitrous oxide (N_2O) in a stoichiometric manner.[13−16] When nitric oxide reacts with phosphine (PH_3) at room temperature, formation of a yellow amorphous powder (not $H_3P{=}O$) on the surface of the reaction container is observed. Interestingly, similar to the case of the black/red phosphorus, the solid material is rather stable in air and water and insoluble in most solvents, including water, acetone, and chloromethanes (CH_2Cl_2 and $CHCl_3$).[16,17] Initial studies reported in the literature indicated that the yellow material was mainly "phosphorus" containing H_3PO_3 and H_3PO_4.[16] A more recent study based on X-ray fluorescence (XRF) measurements has not found considerable amounts of oxygen or nitrogen on the solid material surface.[17] As discussed in detail later in this article measurements performed in the present study combining thermogravimetric analysis and mass spectrometry (TGA-MS) indicate that a large amount of reduced phosphorus in the form of PH_3 and P_4 (as much as 80 wt % in mass of phosphorus) is released from the solid material when the temperature is increased to 873 K in a helium atmosphere. The ratio of the weight loss at the low-temperature regime of 373−673 K (mainly PH_3) to the corresponding weight loss at the high-temperature range of 673−873 K (mainly P_4) indicates a ratio of phosphorus to hydrogen in the solid material of about 1:1.1 (see details in the Experimental Section below), concluding that the material is a novel composite of phosphorus and hydrogen. Our results provide solid experimental evidence supporting the conclusion that the air/water-stable material formed in the reaction of PH_3 and NO is a polyhydride phosphorus polymer [P_xH_y] ($x \approx y$). This conclusion is in excellent agreement with previous proposals in favor of the existence of hydrophosphorus [P_xH_y] polymers, although these compounds have never been systematically prepared and characterized.[18,19]

A very important issue regarding formation of polyhydride phosphorus polymers in the yellow solid material is related to the energetics and mechanism governing the reaction between PH_3 and NO. In previous studies the NO monomer was thought to react with phosphine in a consecutive manner.[14,16] These conclusions are in stark contrast with recent kinetics and theoretical studies that have suggested that the nitric oxide dimer $(NO)_2$ is a more effective oxidant than NO.[6,14,15] In this work we use highly correlated ab initio electronic structure calculations in order to shed some light on the mechanism for the reaction between NO and PH_3. As further discussed in the text, the results show how PH_3 converts to the stable P−P polyphosphine material via phosphine oxide, as illustrated in Scheme 1.

Scheme 1. Proposed Mechanism for Formation of Phosphine Polymer

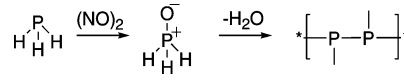

Theoretical Basis

Phosphorus-containing systems remain a major challenge for theoretical calculations due to their complicated electronic structure. For example, it has been debated for a long time whether the nature of the P−O bond in phosphorus oxide is a covalent double (P═O) or an ionic (P^+-O^-) bond.[20] In pioneering work Bocker and collaborators[1] applied a simple theoretical model to determine and classify the structures of a series of covalent phosphorus networks. Major advances in computational algorithms combined with the advent of more powerful computer hardware has allowed scientists to apply ab initio electronic structure calculations to investigate chemical reactions of phosphorus materials such as PH_2 oxidation,[21] predict the stability of phosphorus endohedral cage molecules,[22] as well as estimate binding energies and physicochemical properties of small phosphorus molecules.[23] Recent studies have shown that density functional theory (DFT) is capable of predicting the correct geometry of phosphorus-containing compounds[22] while wrongly estimating the relative energies of some of the isomers.[20] Wesolowski et al. computed the relative energies and conversion barriers of phosphinous acid (H_2POH) to the oxide isomer (H_3PO), evaluating the performance of a series of theoretical methodologies.[20] While numerous theoretical methods exhibit rather large errors (10−240 kJ/mol) in their predicted relative energies,[24−28] the CBS-QB3 model,[29] a variant of the complete basis set (CBS) method originally proposed by Peterson, has been found to produce results with significantly smaller errors (approximately 2.4 kJ/mol; see

(12) Ho, D. G.; Gao, R. M.; Celaje, J.; Chung, H. Y.; Selke, M. *Science* **2003**, *302* (5643), 259–262.
(13) Dobbie, R. C. *J. Chem. Soc. (A)* **1971**, 2894–2897.
(14) Lim, M. D.; Lorkovic, I. M.; Ford, P. C. *Inorg. Chem.* **2002**, *41* (4), 1026–1028.
(15) Zhao, Y. L.; Bartberger, M. D.; Goto, K.; Shimada, K.; Kawashima, T.; Houk, K. N. *J. Am. Chem. Soc.* **2005**, *127* (22), 7964–7965.
(16) Odom, J. D.; Zozulin, A. J. *Phosphorus Sulfur Silicon Relat. Elem.* **1981**, *9* (3), 299–305.
(17) Flora, J. W.; Byers, L. E.; Plunkett, S. E.; Faustini, D. L. *J. Agric. Food Chem.* **2006**, *54* (1), 107–111.
(18) Wiberg, E.; Müller-Schiedmayer, G. *Chem. Ber.* **1959**, *92* (9), 2372–2384.
(19) Corbridge, D. E. C. *The structural chemistry of phosphorus*; Elsevier Scientific Publishing Co.: Amsterdam, New York, 1974; pp xiii, 271−272.
(20) Wesolowski, S. S.; Brinkmann, N. R.; Valeev, E. F.; Schaefer, H. F.; Repasky, M. P.; Jorgensen, W. L. *J. Chem. Phys.* **2002**, *116* (1), 112–122.
(21) Kondo, S.; Tokuhashi, K.; Takahashi, A.; Kaise, M.; Sugie, M.; Aoyagi, M.; Minamino, S. *J. Phys. Chem. A* **1999**, *103* (40), 8082–8087.
(22) Wang, Y. J.; Xu, J. Q.; Cao, Z. X.; Zhang, Q. N. *J. Phys. Chem. B* **2004**, *108* (15), 4579–4581.
(23) Katsyuba, S.; Schmutzler, R.; Grunenberg, J. *Dalton Trans.* **2005**, (9), 1701–1706.
(24) Boatz, J. A.; Schmidt, M. W.; Gordon, M. S. *J. Phys. Chem.* **1987**, *91* (7), 1743–1749.
(25) Cramer, C. J.; Dykstra, C. E.; Denmark, S. E. *Chem. Phys. Lett.* **1987**, *136* (1), 17–21.

ref 29). In the CBS-QB3 method, geometry optimizations, harmonic vibrational frequencies, and zero-point energies (ZPE) are computed with the hybrid exchange-correlation DFT functional B3LYP.[30,31] Using this geometry the energetics are further computed via a series of single-point calculations involving second- and fourth-order Mϕller−Plesset perturbation theory (MP2 and MP4)[32] and quadratic configuration interaction in the space of single, double, and triple electron excitations QCISD(T).[33] The resulting energy is also corrected by an empirical term that depends on the absolute overlap integral ($|S|_{ii} = \int \varphi_i^{\alpha}\, \varphi_i^{\beta}\, d\tau$) and a spin term that depends on the expectation value of the spin ($\langle S^2 \rangle$).[29]

Given that CBS-QB3 provides a good compromise between accuracy and computational speed we adopt this method to compute structures and energies corresponding to all stationary points considered in this work.

Results and Discussion

(a) Oxidation of Phosphine. The optimized structures of the reactants, intermediates, transition states, and products involved in this reaction are depicted in Figure 1. Figure 2 shows a schematic diagram of the energy profile corresponding to the lowest energy reaction path governing the reaction between PH_3 and NO leading to formation of H_3PO, the species expected to participate in the phosphine polymerization reaction. Table 1 lists the reaction enthalpies and barriers corresponding to the reaction $PH_3 + NO \rightarrow H_3PO$ as well as the energetics of the oxidation of some phosphine derivatives by NO and N_2O for comparison purposes. The geometries of the species listed in Table 1 but not shown in Figure 1 are provided in the Supporting Information. In a previous communication we reported the results of our DFT calculations on the dimerization of nitric oxide and its reactions with nucleophiles.[15] The CBS-QB3 calculations performed in this study predict a higher barrier (111 kJ/mol vs 82 kJ/mol) and a more exothermic reaction (319 kJ/mol vs 264 kJ/mol) when compared to out previous DFT results.[15]

As shown in Figure 2 transition structure **4** corresponding to the (4 + 1) pericyclic reaction of the NO dimer and PH_3 constitutes the thermochemical bottleneck for the overall oxidation process. As observed in Figure 1 our calculations predict that the phosphorus atom in **4** exhibits a square-pyramidal coordination. Similar to the (4 + 1) cheletropic reaction between sulfur dioxide and butadiene the lone pair of the phosphine moiety (as SO_2 in the case of SO_2 + butadiene) and a π bond of the NO dimer (as butadiene) are converted into two σ bonds, leading to a dioxadiazaphosphole

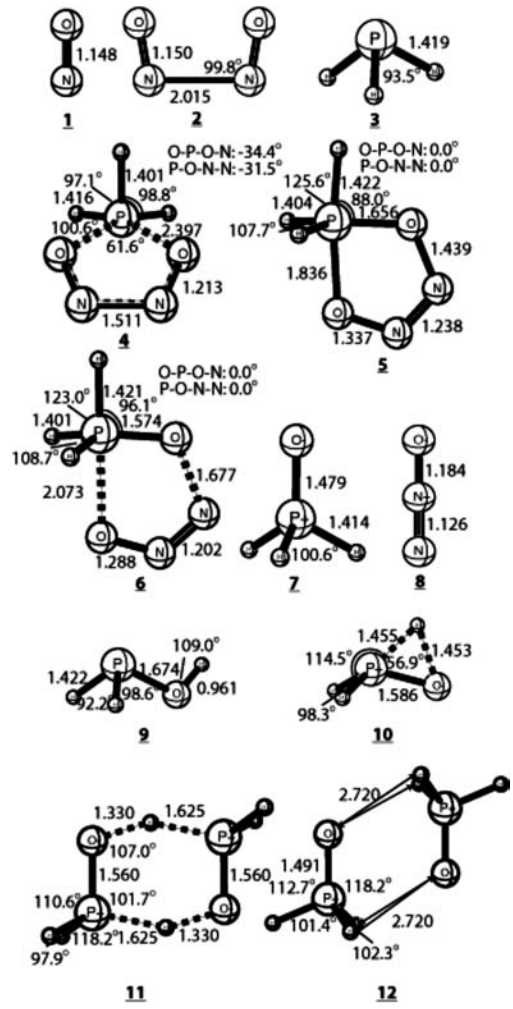

Figure 1. Computed structures of the reactants, intermediates, transition states, and products for the phosphine oxidation and phosphinous acid isomerization (CBS-QB3, distances in Ångstroms).

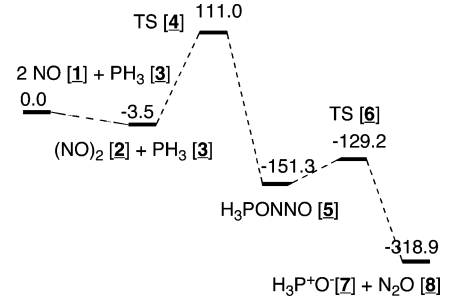

Figure 2. CBS-QB3 reaction energy profile for the lowest-energy pathway of phosphine oxidation (in enthalpy, kJ mol^{-1}).

(**5** in Figure 1) in which the phosphorus atom exhibits a trigonal-bipyramidal coordination and forms two asymmetric P−O bonds with lengths of about 1.656 (equatorial P−O bond) and 1.836 Å (axial P−O bond), respectively. As shown in Figure 2 the resulting adduct (**5**) undergoes a retro-[1,3] dipolar cycloaddition reaction, where the axial P−O bond as well as the longer (and weaker) N−O bond are broken, leading to formation of phosphine oxide, H_3PO, and nitrous oxide, N_2O, (structures **7** and **8** in Figure 1). The reaction was found to be exothermic by approximately 168 kJ/mol and proceed through a transition structure (**6**) that keeps the trigonal-bipyramidal geometry of the phosphorus atom,

(26) Kwiatkowski, J. S.; Leszczynski, J. *Mol. Phys.* **1992**, *76* (2), 475–483.
(27) Kwiatkowski, J. S.; Leszczynski, J. *J. Phys. Chem.* **1992**, *96* (16), 6636–6640.
(28) Chesnut, D. B. *Heteroat. Chem.* **2000**, *11* (1), 73–80.
(29) Montgomery, J. A.; Frisch, M. J.; Ochterski, J. W.; Petersson, G. A. *J. Chem. Phys.* **1999**, *110* (6), 2822–2827.
(30) Becke, A. D. *J. Chem. Phys.* **1993**, *98* (7), 5648–5652.
(31) Lee, C. T.; Yang, W. T.; Parr, R. G. *Phys. Rev. B* **1988**, *37* (2), 785–789.
(32) Møller, C.; Plesset, M. S. *Phys. Rev.* **1934**, *46*, 618–622.
(33) Raghavachari, K.; Trucks, G. W.; Pople, J. A.; Headgordon, M. *Chem. Phys. Lett.* **1989**, *157* (6), 479–483.

Table 1. Reaction Energies and Activation Barriers (in kJ/mol) for the Oxidations of Phosphine and Its Derivatives with the CBS-QB3 Method in the Gas Phase at 298 K[a]

	reaction	ΔH	$\Delta H^{\ddagger}$
a	$2NO \rightarrow (NO)_2$	−3.5	0.0
b	$PH_3 + (NO)_2 \rightarrow H_3PO + N_2O$	−315.6	114.5
c	$PH_2OH + (NO)_2 \rightarrow H_3PO_2 + N_2O$	−411.8	86.1
d	$PH(OH)_2 + (NO)_2 \rightarrow H_3PO_3 + N_2O$	−457.8	69.1
e	$P(OH)_3 + (NO)_2 \rightarrow H_3PO_4 + N_2O$	−463.7	74.4
f	$PH_3 + N_2O \rightarrow H_3PO + N_2$	−290.2	186.1
g	$PH_2OH + N_2O \rightarrow H_3PO_2 + N_2$	−386.4	166.8
h	$PH(OH)_2 + N_2O \rightarrow H_3PO_3 + N_2$	−432.4	152.8
i	$P(OH)_3 + N_2O \rightarrow H_3PO_4 + N_2$	−438.3	148.0

[a] Mean absolute deviation of the CBS-QB3 results is 2.4 kJ/mol for the testing set.[29]

exhibiting a barrier of 22 kJ/mol. Despite our extensive search we were not able to locate the alternative transition state that leads to phosphadioxirane[12,34] and N_2.

(b) Side Reactions of Nitric Oxide and Nitrous Oxide. Table 1 lists the energetics corresponding to the side reactions of nitric oxide and nitrous oxide with a series of phosphorus oxyacids. Reactions of the nitric oxide dimer with the oxyacids (reactions c−e) are predicted to be more exothermic and exhibit lower reaction barriers than the corresponding reactions between nitrous oxide and the same oxyacids (reactions g−i). These results lead to the conclusion that reactions between the dimer $(NO)_2$ and the oxyacids $PH_{3-m}(OH)_m$ ($m = 1-3$) are more thermochemically favorable than those with N_2O due to the fact that donation of an oxygen atom from the N_2O moiety to a three-coordinated phosphorus atom (particularly to PH_3) is a very inefficient process kinetically and not nearly as exothermic as the other processes. The results of our calculations are in good agreement with experimental observations reported by Ford's[14] and Odom's[16] groups, who measured a quantitative yield of 89−95% in the reaction between nitric oxide (NO) with triphenylphosphine (PPh_3)[14] and no reaction at all of PH_3 and N_2O at room temperature.[16] According to our findings it is possible that the net production of N_2 (54%) observed by Odom and Zozulin[16] in the reaction of PH_3 and NO might be the result of reactions between N_2O and downstream products since the multiply hydroxyl-substituted phosphines are more reactive to N_2O: reaction barriers, PH_3 (reaction f) > PH_2OH (g) > $PH(OH)_2$ (h) > $P(OH)_3$ (i) as observed in Table 1.

(c) Isomerization between H_3PO and H_2POH. Given that the yellow powder observed on the surface of the reaction container in the oxidation of PH_3 by NO (see the Introduction above) can be formed in the presence of excess nitric oxide (PH_3:NO = 1:16)[16] it is somehow puzzling to see the lack of formation of phosphoric acid (H_3PO_4) or other reduced oxyacids, especially in view of the thermochemical results obtained in the present work that indicate the feasibility of formation of H_3PO_3/H_3PO_4 (reactions a−e in Table 1). One possible explanation is that four-coordinated phosphines, such as H_3PO and $H_2P(=O)OH$, can only react with nitric oxide (or nitrous oxide) via a two-step mechanism

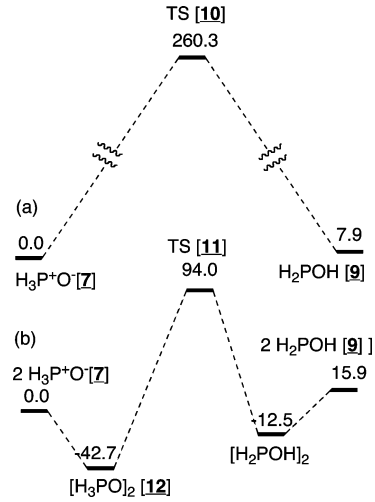

Figure 3. CBS-QB3 reaction energy profile of the two isomerization pathways toward phosphinous acid: (a) concerted and (b) stepwise (in enthalpy, kJ mol^{-1}).

involving a 1,2-hydrogen transfer that leads to formation of the corresponding three-coordinated phosphine derivatives H_2POH and $HP(OH)_2$. Although these species can readily react with NO and N_2O to form H_3PO_4, the overall process is expected to be slow given the unfavorable energetics (small exothermicity and/or large barriers) of the 1,2-hydrogen transfer step.

The gas-phase equilibrium between phosphine oxide and phosphinous acid remains an open question. Calculations using highly correlated ab initio levels of theory predict a small relative energetic difference between the two species in the gas phase (less than ±8 kJ/mol). This result does not seem to be affected by the relative stabilities of the cis and trans conformations of phosphinous acid (trans/cis separation is approximately 0.6 kJ/mol).[20] The gas-phase unimolecular isomerization of H_3PO to H_2POH has been found to exhibit a fairly large reaction barrier (240 kJ/mol calculated at the CCSD(T)/cc-pVTZ level of theory), indicating that this reaction is not feasible in the gas phase.[20,25] These results are in disagreement with conclusions based on indirect experimental evidence supporting the establishment of the equilibrium between the oxide and acid forms.[35−38]

In this work, two possible isomerization pathways have been investigated using the CBS-QB3 method as before: (1) the unimolecular, concerted gas-phase isomerization of H_3PO and (2) the paired, stepwise gas-phase isomerization of H_3PO. The optimized structures of the species involved in these reactions are shown in Figure 1 (**9**−**12**), while the corresponding reaction energy profiles are shown in Figure 3.

As shown in Figure 3a, although the concerted gas-phase isomerization of the oxide to the acid form is slightly endothermic ($\Delta H = 8$ kJ/mol) it exhibits a large reaction barrier ($\Delta H^{\ddagger} = 260$ kJ/mol), indicating that this path is not feasible at room temperature. The large barrier predicted by

(34) Zhao, Y. L.; Houk, K. N. *Abstr. Pap. Am. Chem. Soc.* **2004**, *227*, U157−U157.
(35) Ahmad, I. K.; Ozeki, H.; Saito, S. *J. Chem. Phys.* **1999**, *110* (2), 912–917.
(36) Withnall, R.; Andrews, L. *J. Phys. Chem.* **1987**, *91* (4), 784–797.
(37) Withnall, R.; Andrews, L. *J. Phys. Chem.* **1988**, *92* (16), 4610–4619.
(38) Withnall, R.; Hawkins, M.; Andrews, L. *J. Phys. Chem.* **1986**, *90* (4), 575–579.

our calculations is likely the result of the geometric constraint of the 3-m-r proton transfer with an H−P−O angle of 57° and the antiaromatic 4-electron nature of the cyclic transition state (**10**, also see Figure 1).

Figure 3b shows that the paired isomerization reaction consists of a two-step process where two phosphine oxide moieties attract each other in an exothermic manner (ΔH = −43 kJ/mol) via dipolar interaction, forming the corresponding dimer $[H_3PO]_2$ (**12** in Figure 1). This dimerization reaction is then followed by a "double hydrogen transfer" path where one hydrogen atom bonded to the phosphorus atom on one of the H_3PO moieties is transferred to the oxygen atom of the other H_3PO moiety, forming a H_2POH---H_2POH complex, which further dissociates affording two H_2POH molecules (Figure 3b). The transition structure for this process (**11**) is shown in Figure 1. As observed in Figure 3b, the "double hydrogen transfer" path is endothermic (ΔH_{rxn} = 30 kJ/mol) with an intrinsic barrier of 137 kJ/mol, indicating that the net reaction $2H_3PO \rightarrow 2H_2POH$ is overall endothermic (ΔH = 16 kJ/mol) with a net reaction barrier of 94 kJ/mol. The CBS-QB3 calculations performed in this work suggest that the gas-phase isomerization $H_3PO \rightarrow H_2POH$ is more likely to happen via a stepwise mechanism involving dimerization of H_3PO. Gas-phase isomerization of the oxide to the acid form is slightly less endothermic compared to the calculated isomerization energy of 40 kJ/mol obtained by Wesolowski et al. in aqueous solution.[20]

(d) Condensation of Phosphine Oxide. Although organic phosphine oxides (R_3PO, R = aryl and alkyl) are stable and commercially available as well, H_3PO has only been detected by IR spectroscopy in a very dilute concentration in an argon matrix.[36−38] Not much work has been dedicated to the characterization and elucidation of possible mechanisms governing the condensation reactions (for instance, in concentrated solutions) of H_3PO leading to formation of P−P compounds. A concerted condensation mechanism converting phosphine oxides directly into P−P compounds is highly unlikely given that the four-coordinated phosphorus species is relatively inert. It would seem that any condensation process would have to start with an intermolecular proton transfer that leads to a three-coordinated phosphorus atom such as phosphinous acid (H_2POH) in the case of H_3PO.

We performed CBS-QB3 calculations in order to probe for possible condensation mechanisms involving phosphinous acid, including noncatalytic and autocatalytic reactions. The computed reaction energy profiles as well as optimized structures of some of the species involved in the reactions are shown in Figures 4 and 5, respectively. Other structures discussed and not shown in Figure 4 are shown in the Supporting Information.

As shown in Figure 5a reaction between two H_3PO molecules leading to formation of two molecules of H_2POH is endothermic by 15.9 kJ/mol. The same figure shows that the noncatalyzed condensation between two H_2POH molecules can proceed through two different pathways: one leading to formation of diphosphine ether (**13** in Figure 4) and another leading to formation of hydroxydiphosphine (**14** in Figure 4). CBS-QB3 calculations predict that the first

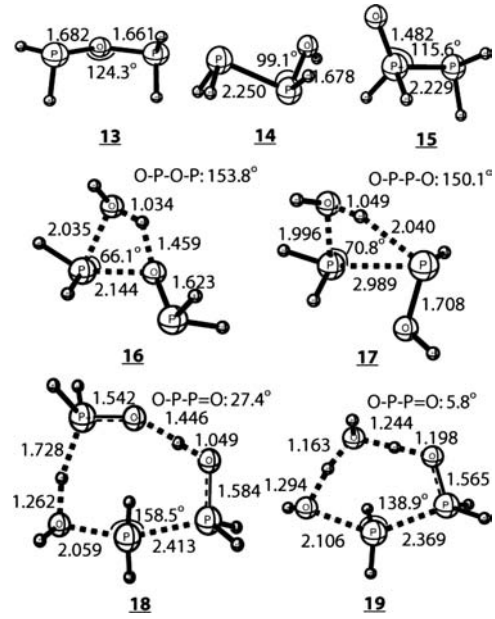

Figure 4. Computed structures of condensation products and transition states (CBS-QB3, distances in Ångstroms).

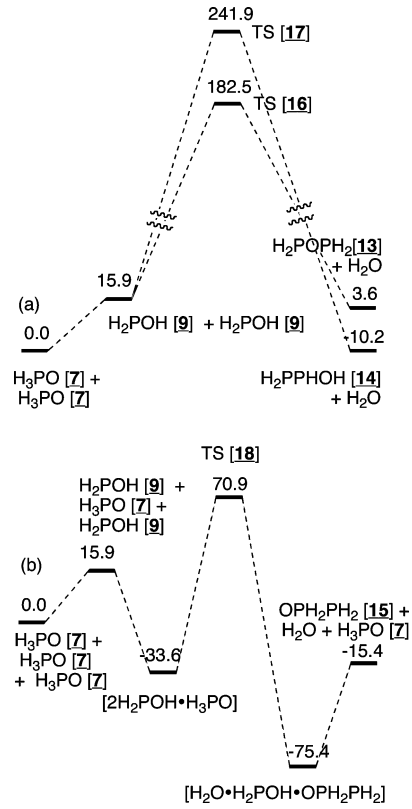

Figure 5. Computed reaction channels toward phosphine ether, acid, and oxide: (a) uncatalyzed and (b) autocatalyzed (CBS-QB3, in enthalpy, kJ mol^{-1}).

pathway is slightly endothermic by 3.6 kJ/mol, while the second is predicted to be exothermic by 10.2 kJ/mol. The same calculations indicate that the barriers (with respect to reactants) for both pathways are predicted to be 183 and 242 kJ/mol, respectively. These relatively high barriers likely result from poor orientation of proton transfers in the transition states (**16** and **17**), which as observed in Figure 4

are characterized by O−P−O and O−P−P angles of 66° and 71°, respectively.

Figure 5b depicts the energy profile of the reaction involving three H_3PO molecules (autocatalytic reaction). The initial step in the reaction involves 1,2-hydrogen transfer in two of the H_3PO that further react with the remaining H_3PO species to form a molecular complex (formed by two phosphinous acids and one phosphine oxide) which lies approximately 34 kJ/mol below reactants. This complex undergoes a condensation process that leads to formation of the hydrated P−P complex [H_2O---H_2POH---OPH_2PH_2] via transition structure (**18**). As observed in Figure 5b this step is exothermic with a heat of reaction of −42 kJ/mol and an intrinsic reaction barrier of 104 kJ/mol. The final step in the reaction involves dehydration of the complex [H_2O---H_2POH---OPH_2PH_2] to produce the P−P compound OPH_2PH_2 and phosphine oxide.

Given the larger exothermicity and considerably lower overall barrier as compared to the two noncatalytic pathways previously discussed, it is reasonable to conclude that condensation of H_3PO is mainly dominated by the catalytic pathway. Regardless of which proton migrates, the two noncatalyzed condensations with relatively high reaction barriers are unlikely to occur at room temperature, probably due to strong 4-electron repulsions between the P atoms that occur when the two species H_2POH approach each other in the vicinity of the transition state. The relatively low reaction barrier obtained for P−P bond formation in the catalyzed condensation (Figure 5b) is likely to be connected to the relatively large O−P−P angle in transition structure **18** (O−P−P = 158°), which favors alignment of the *p* orbitals between the P atoms of the H_2POH moieties and also minimizes steric repulsions in the incipient ring (see Figure 4). We also probed a possible pathway where a water molecule could catalyze the condensation reaction via transition structure (**19**) (Figure 4). The results of our calculations indicate that water seems to be a poorer catalyst, exhibiting a considerably larger reaction barrier (138 vs 71 kJ/mol for the autocatalyzed condensation).

Following the lowest energy P−P formation pathway shown in Figure 5b the nascent phosphine oxide OPH_2PH_2 can further react with another H_3PO molecule to add an additional PH_2 unit in the next cycle of the condensation. This autocatalyzed polymerization can propagate along a reacting network similar to the one shown in Scheme 2, which leads to formation of [P_xH_y] polymers.

(e) Possible Structures of the Polyhydride Phosphorus Polymer. In principle, structures such as cycles, linear coils, branched networks, or dendrimers could be formed from the autocatalyzed polymerization discussed above. In particular, two of the hydrogen atoms in H_3PO could be replaced with R (R = $-P_mH_n$) to control the size and shape of the resulting polymer. Chart 1 shows some possible structures with a phosphorus-to-hydrogen ratio close to 1:1 (which was the P/H ratio determined experimentally in the yellow powder with below TGA-MS measurements).

To determine the most likely structure for the polyhydride phosphorus polymer obtained in the experiment we calculated

Scheme 2. Diagram of the Autocatalyzed Polymerization of Phosphine Oxides

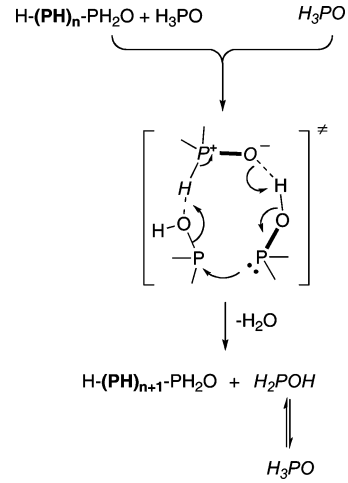

Chart 1. Possible Structures of the Polyhydride Phosphorus Polymer

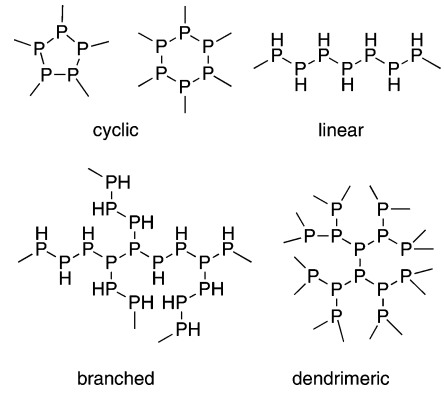

energies for linear and dendrimeric structures of P_4H_6 and $P_{10}H_{12}$ using the B3LYP/CBSB7 method. (Given the large size of both systems they are not computationally tractable at the CCSD(T) or CBS-QB3 levels of theory.) In the case of P_4H_6, the "first-generation phosphine dendrimer" structure was found to be lower in energy than the linear form by 5.2 kJ/mol. When zero-point energy corrections are included this difference drops slightly to 5.0 kJ/mol. In addition, the results indicate that the "second-generation phosphine dendrimer", $P_{10}H_{12}$, is significantly more stable (by 19 kJ/mol) than its corresponding linear isomer. Note that the energy difference per phosphorus atom between the linear and the dendrimeric structure increases as the size of the molecule increases. This is consistent with experimental observations that branched phosphanes generally have higher relative abundance than the corresponding linear isomers.[39]

(f) TGA-MS Analysis. TGA-MS analysis of the yellow material was conducted from room temperature to 1473 K in a helium atmosphere. The results are plotted in Figure 6. The material is thermostable under 373 K and then starts to decompose at high temperature. The mass peaks at m/z = 124, 93, 62, 34, 33, 31, and 2 are signals of fragments of P_4^+, P_3^+, P_2^+, PH_3^+, PH_2^+, P^+ (or P_n^{n+}), and H_2^+, respectively. In the temperature range of 373−573 K a considerable amount of PH_3^+, PH_2^+, P^+, and H_2^+ (H-rich species) were

(39) Baudler, M.; Glinka, K. *Chem. Rev.* **1994**, *94* (5), 1273–1297.

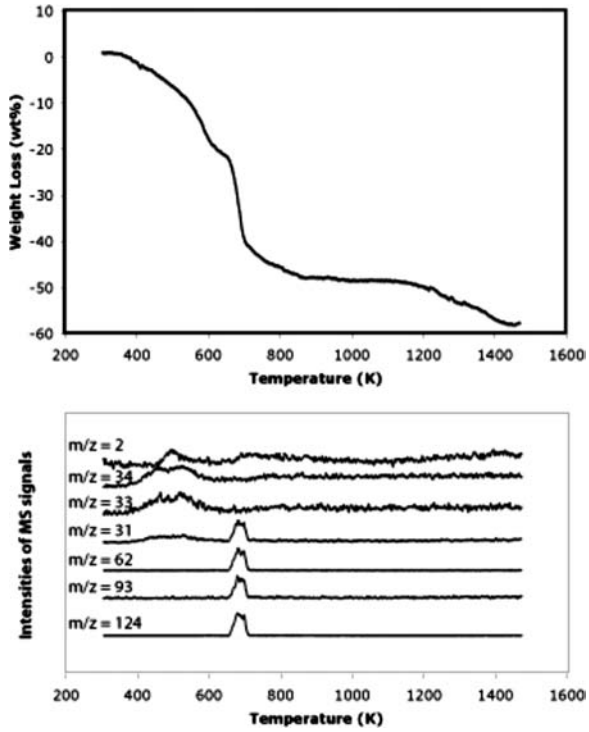

Figure 6. TGA-MS analysis of the yellow solid materials (assignment of MS signals: $m/z = 2$, H_2^+; 34, PH_3^+; 33, PH_2^+; 31, P^+ or P_n^{n+}; 62, P_2^+; 93, P_3^+; 124, P_4^+).

detected with a total weight loss to 20 wt %. Another 30% weight loss occurs at above 673 K, predominantly in the form of P_4. The remaining 50 wt % is likely to be an impurity such as dust (SiO_2), heat-resistant phosphorus pentaoxide P_2O_5 (part of the oxide, ≈10 wt %, can sublime in a form of P_4O_{10} molecule at the high temperature, approximately 1273 K), or both. The low-temperature decomposition at 473 K, which seems to have two stages for $m/z = 33$ and 34 in the MS spectra, may derive from a linear −PH−PH−PH structure and the relatively high-temperature decomposition to tetrahedral phosphorus P_4 at 673 K from the branching structure of P(P<)$_3$. Any pendant P═O groups in the polymer and phosphorus oxyacids impurity would likely be left in the form of P_2O_5 up to 1200 K. The TGA-MS data support our structural analysis of the phosphine polymer.

(g) ATR-FTIR Spectra. The primary IR spectra for the phosphine polymer and phosphoric acid were presented by Flora et al.[17] In this work, attenuated total reflectance Fourier transform infrared (ATR-FTIR) spectra were repeated for the crude sample and isolated solid yellow residue as shown in Figure 7.

It is likely that the surface of the nontreated sample was covered by phosphorus oxyacids formed in the oxidation since the absorptions of the dashed line (Figure 7) were similar to that of H_3PO_4.[17]

It is also possible that the material surface itself was progressively oxidized in air to phosphorus oxyacids. Besides a small amount of the P═O groups left behind after polymerization, additional P═O could be formed by later oxidation of a polyhydride phosphorus polymer, [PH] + [Oxidant] → [P═O] + H_2O.

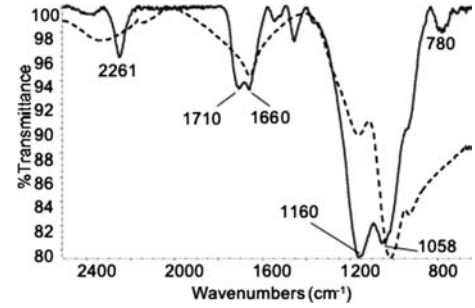

Figure 7. ATR-FTIR spectra of raw product (dashed line) and isolated yellow solid material with cleanup surface (solid line).

Table 2. Comparison of the Gas-Phase Vibrational Frequencies of Phosphine Oxides Computed with the B3LYP/CBSB7 Method and Experimentally Available Data

	computed	exp.
H_3PO	1266 (P═O) 2386 (P−H)	1240 (P═O)
$OP(PH_2)_3$	1203 (P═O) 2390 (P−H)	
$OP(OH)_3$	1319 (P═O)	
$OPH(PH_2)_2$	1209 (P═O)	
$OPH(OH)_2$	1309 (P═O) 2537 (P−H)	1299 (P═O) 2487 (P−H)
OPH_2PH_2	1232	
$OPH_2(OH)$	1292	
$P_{11}H_3$	2260 (P−H)	

In the literature the IR absorptions of P═O groups have been reported to be very strong in the range of 1050−1450 cm^{-1}, dependent on the phosphorus substitutions.[40] The calculated spectra for small phosphorus molecules in the gas phase are consistent with previously reported data within an error of 30 cm^{-1} as shown in Table 2.[36] Compared to the frequency for the P═O group in H_3PO, $-PH_2$ substitution on the phosphorus causes a red shift of about 34−63 cm^{-1} while −OH substitution in the oxyacids causes a blue shift of about 26−53 cm^{-1} due to the difference in electronegativity between phosphorus and oxygen.

Since the P═O groups in the condensed phase take part in formation of hydrogen bonds, the P═O stretching absorption of phosphoric acid red shifts to 1100−1300 cm^{-1} in both the spectra (solid and dashed lines), severely overlapping the possible absorption band of H−P−H bending vibrations. Hydrogen-bond formation within the polymer and phosphoric acid complicates - determination of the phosphorus substitution effects. Owing to electronegative phosphine substitutions, the absorptions for H−O−P bending and P−O stretching both red shift by 50−100 cm^{-1} compared to the values for phosphoric acid (about 1000 and 900 cm^{-1}, respectively).

In the ATR-FTIR spectrum of the yellow materials cleaned by solvents (the solid line in Figure 7) a new absorption at 2261 cm^{-1} is observed, which is the typical signal for the stretching vibration modes of H−P in the polyhydride phosphorus polymer [P_xH_y]. As shown in Table 2, the calculated P−H vibration of $P_{11}H_3$ is located at 2260 cm^{-1}. In addition, new absorptions at 870, 670, and 550 cm^{-1} (see Supporting Information) are likely to be the result of multiple bending vibration modes of H−P−P.

(40) Halmann, M. M. *Analytical chemistry of phosphorus compounds*; Wiley-Interscience: New York, 1972.

Conclusion

We investigated phosphine polymerization initiated by nitric oxide oxidation experimentally and theoretically. On the basis of these results we suggest the following plausible mechanism for formation of the polyhydride phosphorus polymer [P_xH_y]: (a) oxidation of phosphine PH_3 by nitric oxide leads to formation of phosphine oxide H_3PO; (b) competing with continued oxidation to phosphorus oxyacids, phosphine oxide aggregation via dipole−dipole interactions; (c) with the autocatalytic reaction, the phosphine oxides chemically link together via P−P bond and loss of side product water. The overall barriers for polymerization are about 111−113 kJ/mol.

The proposed mechanism is consistent with the following experimental results: (a) XRF cannot detect substantial oxygen on the isolated yellow materials, (b) TGA-MS shows that the elemental ratio of phosphorus and hydrogen is close to 1:1, (c) ATR-FTIR shows that a remarkable amount of phosphorus oxyacids cover the crude yellow material surface, (d) an important absorption in ATR-FTIR of the isolated solid portion corresponds to the new P−H stretching vibration on the P−P skeleton, and (e) in the previous ^{31}P NMR by Odom et al. the original sample ("phosphorus-containing H_3PO_3 and H_3PO_4") may be the crude materials from PH_3 plus NO either.

Among the possible polyhydride phosphorus polymer structures we suggested that the dendrimer is the most likely structure: (a) the core portion of the polymer has a stable skeleton like red and black phosphorus, inert to air and water, (b) $-PH_2$ terminating ends on the dendrimer are relatively more sensitive to environment and could be slowly oxidized to oxyacids and thereby peeled down, and (c) pyrolysis of the materials shows the weak bonding $-PH_2$ ends are dropped at a relatively low temperature (<673 K).

Water effects on polymerization are multiple and complicated in each stage: (a) at the oxidation step water helps to decrease the isomerization barrier between the oxide and acid form, accelerating the deep oxidation toward the phosphorus oxyacids; however, the acid form is less favored in aqueous solution; (b) at the condensation step water catalyzes the reaction less efficiently than phosphine oxide does; furthermore, as a product of the condensation, increasing water amount will inhibit polymerization. Overall, water may promote formation of phosphorus oxyacids but is unlikely to serve polymerization.

The multiple reaction channels computed in Figure 5 can explain the unexpected stability of the P−P materials. First, P−P bond formation is thermodynamically favored with respect to H_3PO. Once all monomer (H_3PO) is consumed the resulting P−P compounds are relatively stable in water; the reverse reaction of hydrolysis has a barrier of 170 kJ/mol, higher than polymerization by 60 kJ/mol. Thus, the polyhydride phosphorus polymer [P_xH_y] could be a stable source of PH_3 at 473 K and P_4 at 673 K. The detailed structures and potential technological applications of the polymer are still to be fully elucidated.

Experimental Section

Computational Methodology. To explore how phosphine polymerization occurs a series of model calculations were conducted to mimic the oxidation, precipitation, and condensation processes. Optimized geometries of reactants, products, transition states, and reaction intermediates were obtained with the DFT level of theory using the B3LYP[30,31] functional and CBSB7 basis set in GAUSSIAN 03 (G03).[41] This is a robust calculation method for a variety of organic reactions, although energetics with this method are disputed for the second-row atoms, e.g., sulfur and phosphorus.[42]

Experimental Details. (a) Material. Polymerization is detailed in a previous publication.[17] In summary, the polyhydride phosphorus polymer was generated in conjunction with phosphorus oxyacids at ambient conditions in 0.2 m^3 (8 ft^3) Plexiglas chambers. These chambers contained approximately 6 kg of a fresh reconstituted tobacco packed in semipermeable containers (e.g., cardboard boxes). An aluminum dish containing 0.8 g of magnesium phosphide (Magtoxin, Degesch, USA) was added to these chambers releasing approximately 1200 ppm PH_3 within about 3 h. Yellow deposition was noted after 24 h of exposure. The residues were also generated by addition of 2.4% nitric oxide (NO) in nitrogen gas (BOC Gases, Richmond, VA) to empty cardboard boxes or boxes containing flue-cured tobacco in the presence of approximately 1200 ppm PH_3. NO was added in three 1-min increments at a 1 L/min flow rate.

The yellow residue formed in the above reaction was rinsed from the 0.2 m^3 chamber with methanol. Fifty milliliter aliquots were dispensed into centrifuge tubes and centrifuged for 2 min at 209 $rad \cdot s^{-1}$. Methanol was decanted, and the yellow solid was twice rinsed with water, centrifuged, and water decanted. Samples were then rinsed twice with acetone followed by centrifugation and removal of acetone. The solid yellow material was dried under a stream of nitrogen gas.

(b) TGA-MS. A 10 mg amount of yellow powder was put into the sample pan of a Netzsch STA409 Skimmer thermogravimetric analyzer with an electron-impact quadrupole mass-selective detector. Using helium as carrier gas, the mass signals were collected at m/z = 2, 31, 33, 34, 62, 93, and 124 from room temperature to 1473 K with a temperature-increase rate of 20 K/min.

(c) Infrared Spectroscopy. Fourier transform infrared spectroscopy (FT-IR) analysis was conducted using a Thermo Nicolet (Madison, WI) Nexus 670 ESP equipped with an attenuated total reflectance (ATR) unit, Smith Detection (Raleigh, NC) single-bounce Durascope with a diamond crystal. Samples were collected using 64 scans, 4 cm^{-1} resolution, and Happ-Genzal apodization.

(41) Frisch, M. J.; Trucks, G. W.; Schlegel, H. B.; Scuseria, G. E.; Robb, M. A.; Cheeseman, J. R.; Montgomery, J., J. A.; Vreven, T.; Kudin, K. N.; Burant, J. C.; Millam, J. M.; Iyengar, S. S.; Tomasi, J.; Barone, V.; Mennucci, B.; Cossi, M.; Scalmani, G.; Rega, N.; Petersson, G. A.; Nakatsuji, H.; Hada, M.; Ehara, M.; Toyota, K.; Fukuda, R.; Hasegawa, J.; Ishida, M.; Nakajima, T.; Honda, Y.; Kitao, O.; Nakai, H.; Klene, M.; Li, X.; Knox, J. E.; Hratchian, H. P.; Cross, J. B.; Bakken, V.; Adamo, C.; Jaramillo, J.; Gomperts, R.; Stratmann, R. E.; Yazyev, O.; Austin, A. J.; Cammi, R.; Pomelli, C.; Ochterski, J. W.; Ayala, P. Y.; Morokuma, K.; Voth, G. A.; Salvador, P.; Dannenberg, J. J.; Zakrzewski, V. G.; Dapprich, S.; Daniels, A. D.; Strain, M. C.; Farkas, O.; Malick, D. K.; Rabuck, A. D.; Raghavachari, K.; Foresman, J. B.; Ortiz, J. V.; Cui, Q.; Baboul, A. G.; Clifford, S.; Cioslowski, J.; Stefanov, B. B.; Liu, G.; Liashenko, A.; Piskorz, P.; Komaromi, I.; Martin, R. L.; Fox, D. J.; Keith, T.; Al-Laham, M. A.; Peng, C. Y.; Nanayakkara, A.; Challacombe, M.; Gill, P. M. W.; Johnson, B.; Chen, W.; Wong, M. W.; Gonzalez, C.; Pople, J. A. *Gaussian 03*, Revision C.02; Gaussian, Inc: Wallingford, CT, 2004.

(42) Zhao, Y. L.; Jones, W. H.; Monnat, F.; Wudl, F.; Houk, K. N. *Macromolecules* **2005**, *38* (24), 10279–10285.

Acknowledgment. Y.L.Z., W.D.T., and S.L.G. are INEST fellowship recipients (INEST, Interdisciplinary Network of Emerging Science and Technology). The authors thank the INEST group for support and NIST and NIH for administration and supercomputer time. Partial calculations were conducted in NIH Biowulf cluster. The synthesis and FTIR experiments were conducted by J.W.F. and TGA-MS by W.D.T. Certain commercial materials and equipment are identified in this paper in order to specify procedures completely. In no case does such identification imply recommendation or endorsement by the National Institute of Standards and Technology nor does it imply that the material or equipment identified is necessarily the best available for the purpose.

Supporting Information Available: Geometries for all structures discussed in the paper. This material is available free of charge via the Internet at http://pubs.acs.org.

IC801917A